forests

MDPI

Article

Dendrochronology-Based Normalized Difference Vegetation Index Reconstruction in the Qinling Mountains, North-Central China

Jin Qin [1], Hongying Bai [2,*], Pei Zhao [1], Shu Fang [1], Yuanlin Xiang [2] and Xiaoyue Huang [2]

[1] College of Urban, Rural Planning and Architectural Engineering, Shangluo University, Shangluo 726000, China; jearkeens@163.com (J.Q.); pzhao@imde.ac.cn (P.Z.); 201930@slxy.edu.cn (S.F.)
[2] Shaanxi Province Key Laboratory of Earth Surface System and Environmental Carrying Capacity, Northwest University, Xi'an 710127, China; xbdxiangyuanlin@126.com (Y.X.); huangxiaoyue1228@163.com (X.H.)
* Correspondence: hongyingbai@163.com

Abstract: *Larix chinensis* Beissn., as a native, dominant and climate-sensitive coniferous species at Mount Taibai timberline, Qinling mountains, is rarely disturbed by anthropogenic activities; thus, it is an ideal proxy for the investigation of climate change or vegetation evolution. In this study, we applied dendrochronological methods to the *L. chinensis* tree-ring series from Mt. Taibai and investigated the relationships between tree-ring widths and NDVI/climate factors using Pearson correlation analysis. On the basis of the remarkable positive correlations ($r = 0.726$, $p < 0.01$, $n = 23$) between local July normalized difference vegetation indices (NDVI) and tree-ring width indices, the regional 146-year annual maximum vegetation density was reconstructed using a regression model. The reconstructed NDVI series tracked the observed data well, as the trans-function accounted for 52.8% of observed NDVI variance during AD 1991–2013. After applying an 11-year moving average, five dense vegetation coverage periods and six sparse vegetation coverage periods were clearly presented. At a decadal scale, this reconstruction was reasonably and negatively correlated with a nearby historical-record-based dryness/wetness index (DWI), precisely verifying that local vegetation cover was principally controlled by hydrothermal variations. Spectral analysis unveiled the existence of 2–3-year, 2–4-year, 5–7-year and 7–11-year cycles, which may potentially reflect the connection between local NDVI evolution and larger-scale circulations, such as the El Niño–Southern Oscillation (ENSO) and solar activity. This study is of great significance for providing a long-term perspective on the dynamics of vegetation cover in the Qinling mountains, and could help to guide expectations of future forest variations.

Keywords: *Larix chinensis* Beissn.; timberline; tree-ring width; NDVI reconstruction; climate response

check for updates

Citation: Qin, J.; Bai, H.; Zhao, P.; Fang, S.; Xiang, Y.; Huang, X. Dendrochronology-Based Normalized Difference Vegetation Index Reconstruction in the Qinling Mountains, North-Central China. *Forests* **2022**, *13*, 443. https://doi.org/10.3390/f13030443

Academic Editor: Pavel A. Moiseev

Received: 26 January 2022
Accepted: 10 March 2022
Published: 11 March 2022

Publisher's Note: MDPI stays neutral with regard to jurisdictional claims in published maps and institutional affiliations.

Copyright: © 2022 by the authors. Licensee MDPI, Basel, Switzerland. This article is an open access article distributed under the terms and conditions of the Creative Commons Attribution (CC BY) license (https://creativecommons.org/licenses/by/4.0/).

1. Introduction

Terrestrial ecosystems have undergone significant changes with the intensification of global warming; therefore, the response of terrestrial ecosystems to global climate change has become one of the major concerns of various scientific communities [1]. As an essential component of terrestrial ecosystems, vegetation not only sensitively responds to climate change, but is also a comprehensive indicator for monitoring land-surface ecosystems and environments [2]. Thus, with the development of remote sensing in the past decades, there has been significant growth in research involving the monitoring of vegetation coverage variation and land-cover change [3,4].

The normalized difference vegetation index (NDVI), determined by the ratio between near-infrared (λ = 0.7–1.1 mm) and red (λ = 0.6–0.7 mm) of the electromagnetic spectrum, is an ideal and widely applied source to indicate the temporal and spatial changes in vegetation coverage and productivity [5,6]. NDVI has been constantly utilized to describe the state

of vegetation growth because it provides abundant signals for global eco-environmental detection [7]. In China, NDVI was used to detect phenological changes, classify large-scale vegetation and estimate vegetation biomass in response to climate change and its feedback [8]. However, instrumental and historical vegetation records worldwide were very limited before the 1980s, and hardly met the needs of long-term vegetation variability investigation. Thus, further understanding historical vegetation dynamics is critical for local environmental management.

Tree-ring width records, a natural proxy for historical climate change study, are frequently employed because of their high resolution, relatively low dating errors, wide distribution and explicit indication of climate change [9]. Former studies discovered that tree-ring series convey key information about interactions between vegetation growth and the environment by archiving clear signals of environmental influences on the ecosystem over time [10,11], and tree-ring width indices based on samples collected in arid, semi-arid and semi-humid areas of East Asia are significant for reconstructing the climate change in these regions [12]. Additionally, many studies have found that tree rings are a good proxy for reconstructing historical vegetation dynamics because there exists a significant correlation between tree radial growth variations and NDVI dynamics [13,14].

The Qinling Mountain range, lining from east to west, is a famous demarcation line between the semi-humid and semi-arid areas of China and acts as a giant block for monsoon air streams [15]. As one of the most representative ecological transition zones in north-central China, as well as the area in which natural resources are concentrated, dendrochronological study of this area has rapidly developed during recent decades, bringing about a number of achievements [16,17]. However, previous research mainly focused on climate change reconstruction and the radial-growth–climate relationship; there are scarce reports about reconstructing historical NDVI variability by utilizing dendrochronological techniques around the Qinling mountains. Hence, it is crucial to explore the capability of NDVI reconstruction by utilizing tree rings, and to display greenness coverage variation in the Qinling mountains.

Mt. Taibai, the highest peak of the Qinling mountains and the water source catchment of the Heihe River, serves as the source of headwaters for Xi'an City, one of the largest cities in north-central China. The ecosystem services of Mt. Taibai influence not only the wildlife of the surrounding mountainous areas, but also the social and economic development of the adjacent populated areas. Reconstructing Mt. Taibai timberline vegetation dynamics is of practical significance for studying local ecological and environmental evolutions under the framework of global change. To increase the knowledge of NDVI fluctuations in Mt. Taibai, as well as the potential influences on environmental changes, and to extend the network of tree-ring chronologies in Qinling mountains, we utilized the *Larix chinensis* Beissn. tree-ring proxy to reconstruct the NDVI variations. The aims of this article are to: (1) identify the relationship among *L. chinensis* tree ring widths, the NDVI covering Mt. Taibai, and surrounding climate conditions; and (2) unveil the potential of NDVI reconstruction by using a tree-ring proxy and recover the vegetation evolution of Mt. Taibai over the last century. These studies will be important references to help us understand the local vegetation and the aspects of ecosystem evolution that depend on it, as well as efficient forest utilization and reasonable administration under the background of global change.

2. Materials and Methods

2.1. Site Description

Mt. Taibai (33°49′–34°10′ N, 107°19′–107°58′ E), located southwest of Xi'an city in Shaanxi province, north-central China, is the highest mountain to the east of the Tibetan plateau and plays an important role in both geographical and cultural status (Figure 1). There are more than 15 categories of second- and third-tier protected plant species, about 40 species of animals, 230 species of birds, and several species of amphibians. Mt. Taibai has become a National Nature Reserve covering an area of 56,325 ha (1 ha = 10,000 m^2) since 1986, in order to preserve its intact ecosystem [18]. Mt. Taibai possesses a typical continental

monsoon climate with arid, cold winters and humid, hot summers. The mean annual temperature and rainfall (the heavy rain season is from June to August) at the top of Mt. Taibai are around 2 °C and 800–900 mm, respectively, and both the maximum temperature and most intense rainfall have always been documented in July. Such climate conditions are conducive to plant growth and water utilization, which guarantee physiological activities and improve the efficiency of nutrient and mineral transmission during the carbohydrate synthesis of plants, with enough supplementation from soil moisture.

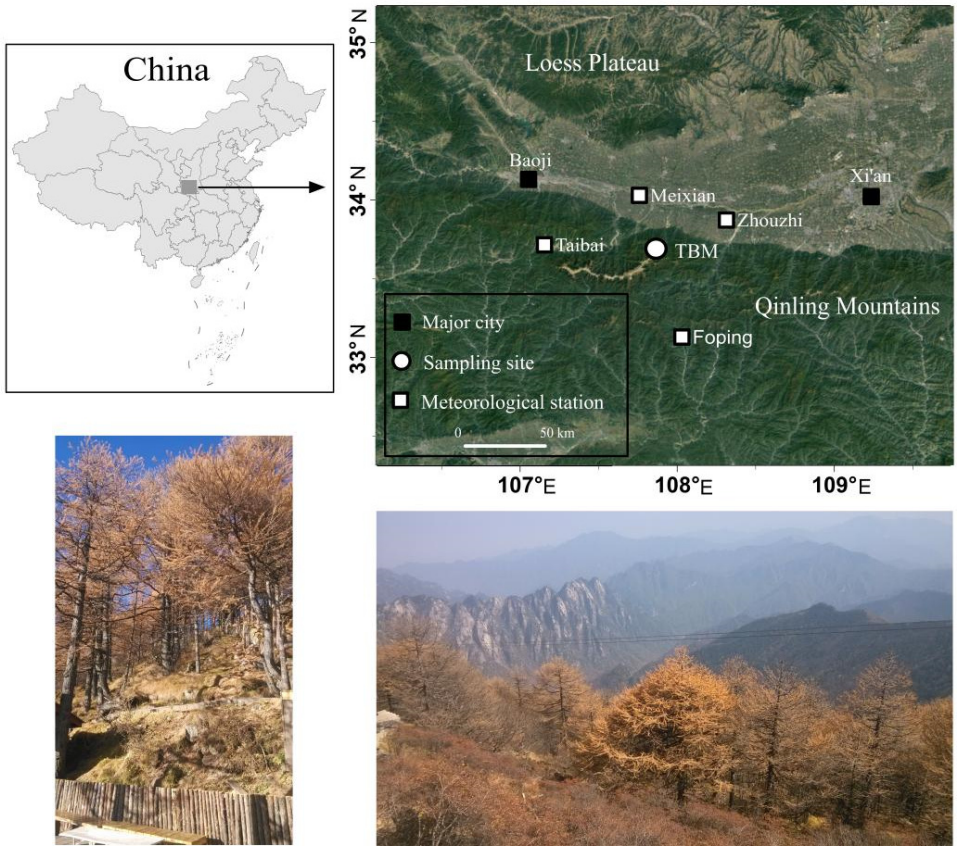


Figure 1. Location of the sampling site and surrounding meteorological stations. Black squares represent cities, white circles represent sampling sites, and white squares represent meteorological stations. Google © is the source of satellite image.

The vegetation is of remarkable vertical distribution, with deciduous broad-leaved forests, mixed conifer–deciduous forests, conifer forests, and sub-alpine meadows, from low elevation to the mountain top. Specifically, a wide range of Quaternary glacial remnants and sub-alpine meadows (e.g., *Rhododendron capitatum* Maxim.) are distributed above 3400 m a.s.l. *L. chinensis* is a dominant or co-dominant species along the elevational gradient within 3000 and 3500 m a.s.l.; the soil type is mountain podzolic brown forest soil; and the thickness of soil layer is 10–30 cm. Below the lower limit of *L. chinensis* forests, *Abies fargesii* Franch forests cover an elevation of 2500–3000 m a.s.l.

2.2. Tree-Ring Data

In October of 2013, radial increment cores of *L. chinensis* were collected along the gradient of the northern aspect of Mt. Taibai at an elevation of 3062–3403 m a.s.l., where large stretches of dominant *L. chinensis* forests emerged (Figure 1). The slope angle ranged from 15° to 45°.The sampling site code was named TBM (Taibai Mountain), which was 2 km away from the peak. Natural forests with thin soil layers, large slopes, good tree growth, and no pests or diseases were selected for sample collection according to the International Tree-Ring Data Bank (ITRDB) standard [19], and two cores from perpendicular directions

at the breast height of each given isolated-living tree were originally extracted with increment borers. Finally, 50 tree cores from trees in a homogeneous micro-environment were gathered.

Step-by-step, all of the tree-ring samples were air-dried, glued, fixed and mounted in the slots of wood planks according to conventional preprocess methods [20]. The accurate calendar year of each individual ring was identified after visual cross-dating under microscopy. Then, each annual ring width within a 0.001 mm resolution was measured using a LINTAB system. After that, the cross-dating results were further quality-controlled on a COFECHA computer program [21] which produces statistical references for sample selection or chronology construction. After optimization, 46 tree-ring series were conserved in total. All the individual growth series were standardized on ARSTAN [22] to remove the non-climatic trends and preserve more climate-related signals using the negative exponential function. To eliminated age-related biological growth trends from each tree-ring series, a cubic spline with a 50% response cut-off at the half-length of the series was applied. The standard chronology was determined by calculating the bi-weighted robust means of detrended data from individual tree cores. Since standardized series usually contain autocorrelation that negates the assumption of independence [23,24], we removed the effects of autocorrelation by transforming each standardized series into residual series through pooled autoregressive modeling [25]. Thus, standard (STD) and residual (RES) chronologies were established (Figure 2).

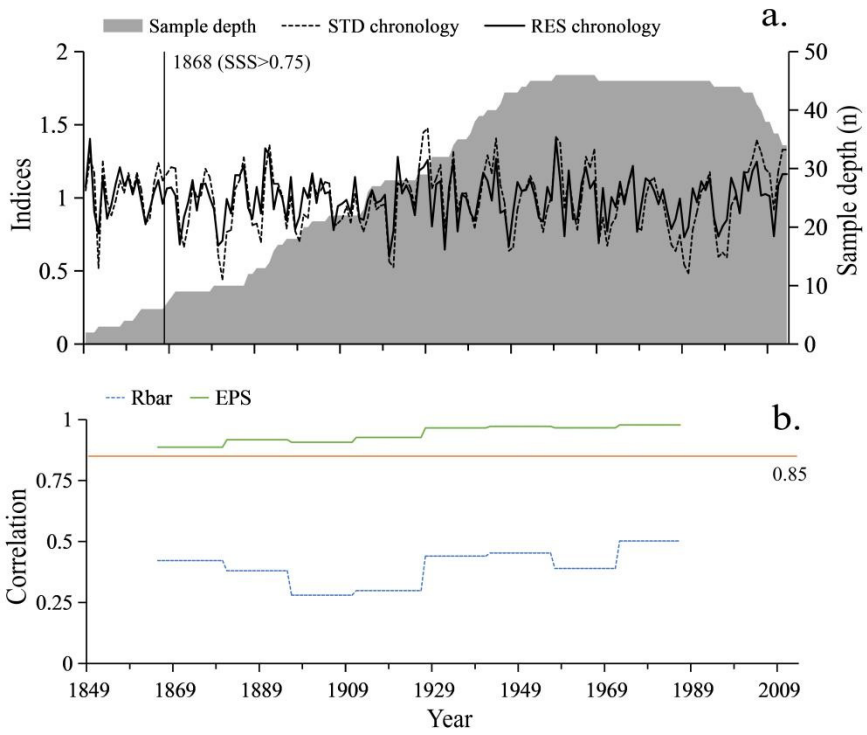


Figure 2. The curves of residual chronology (RES), standard chronology (STD) and sample depth (**a**). The EPS (expressed population signal, blue line) and Rbar (average correlation between series, green line) over a 30-year running window with 15-year overlaps (**b**). Rbar ranges from 0.28–0.50, EPS ranges from 0.88–0.98. EPS value is higher than 0.85 from 1865. The vertical line indicates that the acceptable (valid) time for tree-ring width chronology for estimation starts at 1868 (SSS > 0.75). The orange horizontal line is the 0.85 cutoff for EPS.

2.3. Meteorological Data and NDVI Datasets

Meteorological data: The instrumental meteorological records at the common duration of AD 1959–2013, consisting of monthly mean temperature and total precipitation, were derived from 4 adjacent county-located lower-land stations (Meixian, Zhouzhi, Taibai

and Foping; Figure 1, Table 1), which represented the climatic conditions of the northern, western, eastern and southern aspects of Mt. Taibai, respectively.

Table 1. Description of the meteorological stations around Mt. Taibai.

Code	Meteorological Station	Latitude (°N)	Longitude (°E)	Altitude (m a.s.l.)
1	Zhouzhi	34.2	108.2	433.1
2	Meixian	34.3	107.8	517.6
3	Foping	33.6	108.0	1087.7
4	Taibai	34.1	107.3	1543.6

As the altitude rose, there was an obvious pattern in temperature lapse along the gradient (Figure 3a). Monthly mean temperatures among the 4 stations were positively correlated with each other (r = 0.528–0.944, $p < 0.01$) and the same can be said for monthly mean total precipitation (r = 0.447–0.946, $p < 0.01$). The research area experienced the most abundant rainfall from July to September (Zhouzhi: 293.16 mm; Meixian: 303.13 mm; Foping: 496.53 mm; Taibai: 398.53 mm; accounting for 50.32%, 54.68%, 54.84% and 54.13% of the whole year, respectively), while the highest temperature mainly occurred from June to August (Zhouzhi: 25.3 °C; Meixian: 24.6 °C; Foping: 21.3 °C; Taibai: 18.1 °C); these are characteristic of a continental monsoon climate.

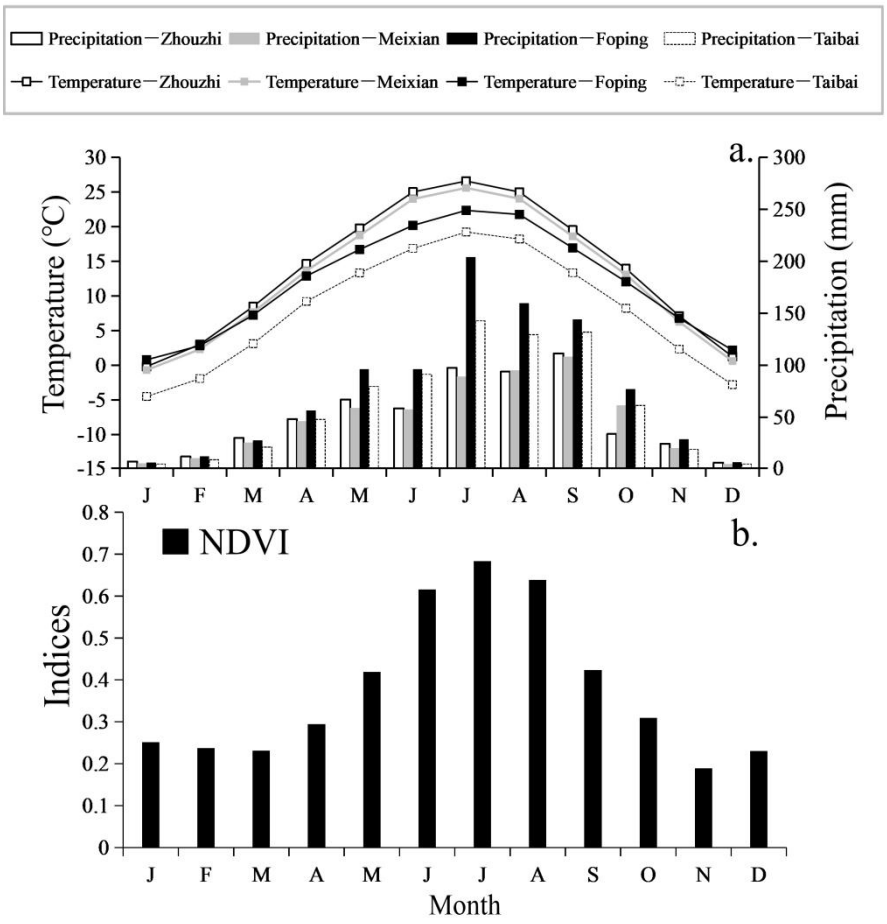


Figure 3. Monthly variation of mean air temperature and total precipitation for Foping, Meixian, Zhouzhi and Taibai county in AD 1959–2013 (**a**), and changes in average monthly TBM NDVI in AD 1991–2013 (**b**).

NDVI data: Monthly NDVI data were obtained using the international general Maximum Value Composite (MVC) method. When the NDVI value exceeds 0.1, it means that

there is vegetation coverage, and the higher NDVI value, the higher the vegetation coverage rate will be. The satellite records of monthly changes in terrestrial vegetation covering the study area (34°0′ N, 107°42′ E) from two separate sources were combined over the observation period of 1991–2013 according to the following steps. Firstly, the latest monthly 250 m × 250 m MODIS VGT-NDVI datasets covering 2000–2013 were collected from the "Eco-decade project in Shaanxi Province" datasets, which had already been processed with atmospheric, radiometric and geometric corrections [26]. Secondly, the 8 km × 8 km global NDVI datasets (Royal Netherlands Meteorological Institute's Data-sharing System, http://climexp.knmi.nl, accessed on 4 January 2016) based monthly NDVI throughout AD 1982–2000 were extracted. There was a great departure in the resolution and the scale of plant distribution coverage between the two datasets (the 8 km × 8 km resolution covered most of the botanical distributions, whereas the 250 m × 250 m resolution may have only covered the *L. chinensis* and sub-alpine meadows), and previous research revealed that 1990 was one of the three most extreme wet events during AD 1852–2016 [27], which may result in inaccurate correlation between NDVI and tree rings. Therefore, we only selected the 8 km × 8 km resolution monthly NDVI data between AD 1991–2000, with the aim of prolonging the 250 m × 250 m resolution data. Finally, we combined the high-resolution data with the low-resolution data for the time period of AD 1991–2013 as TBM NDVI via normalization.

2.4. Statistical Analysis

Firstly, we performed a Pearson correlation analysis between tree-ring width chronology and the monthly average temperature and precipitation of the four surrounding meteorological stations, to study the relationship between tree radial growth and climatic factors. Secondly, to investigate the NDVI–tree radial growth relationship, we analyzed the Pearson correlation between tree-ring width chronology and TBM NDVI. Thirdly, to explore the relationship between surrounding climate variables and vegetation coverage, we conducted a Pearson correlation analysis between the selected monthly NDVIs and meteorological data. Considering the possible lagging effect of climatic factors on vegetation coverage and on tree radial growth, we defined the beginning observation month as the previous September.

Hence, a trans-function conveying of the mathematical relationship between tree-ring width chronology and TBM NDVI was established through linear regression analysis, and used to reconstruct the vegetation dynamics over the periods available. The fidelity of the trans-function was examined using leave-one-out cross-validation [28], which was used to test the model's stability and reliability. The testing statistics included the explained variance (R^2), the adjusted explained variance (R^2_{adj}), correlation coefficient (r), reduction of error (RE), product mean test (t), sign test ($S1$), first difference sign test ($S2$), variance test value (F) and Durbin–Watson value (D/W). To assess the vegetation variability at a regional scale and indicate the hydrothermal history of Mt. Taibai, we examined the coherence of the reconstructed NDVI series with the adjacent (Baoji city (Figure 1)) dryness/wetness index (DWI); this was based on historical documents and used to assess the humid conditions of a specific region, as well as the conditions of flood, water logging, normal, dry and severely dry as degrees of 1, 2, 3, 4 and 5, respectively [29]. All of the above statistical calculations were carried out using SPSS software. Wavelet analysis was performed using Matlab R2014a to decompose time series into temporal and spatial space and identify the main time series periods, as well as their changes with time [30]. We applied an 11-year lower-pass Fast Fourier Transformation filter to display the multi-decadal variations of the reconstructed NDVI.

3. Results

3.1. Monthly Variation Characteristics of Mt. Taibai NDVI

Overall, obvious uni-modal variation was demonstrated from the Mt. Taibai monthly NDVI (TBM NDVI) (Figure 3b), with relatively stable values from January to March and

from November to December, but relatively variable values from May to September. NDVI was at its lowest level during spring and winter, indicating an absence or low percentage of evergreen species maintaining green foliage during dormancy. No rising trend was found during January to March, but values maximized at 0.68 in July after April with a remarkable increase, indicating that the presence of green foliage occurs at the most flourishing stage of a year. The vegetation basically ceased to grow, even though the NDVI of September was relatively high. Similarly to other findings, vegetation growth in Mt. Taibai mainly occurred in summer (June–August) [31,32].

3.2. Descriptive Statistical Characteristics of Chronologies

The statistical characteristics of the chronologies are summarized in Table 2.

Table 2. Summary of statistics for *Larix chinensis* tree-ring residual chronology (RES) and standard chronology (STD) of Mt. Taibai.

Statistical Item	RES	STD
Mean sensitivity	0.22	0.19
Standard deviation	0.19	0.21
First-order autocorrelation	0.02	0.51
Variance in first eigenvector (%)	50	54
Signal–noise ratio	12.15	10.44
Mean correlation within a tree	0.62	0.60
Mean correlation between trees	0.49	0.48
Expressed population signal	0.94	0.92
Length/a	165	165
First year where SSS > 0.75 (No. cores)	1868 (7)	1870 (9)

Mean sensitivity is a key parameter indicating obvious year-to-year variation in tree-ring width and closely related to local climate variations [33]. The values both exceed the threshold of 0.14 in RES chronology (0.22) and STD chronology (0.19), indicating strong environmental fluctuation signals in *L. chinensis* tree ring widths. The variance in the first eigenvectors of the chronologies are very close, that is, 50% (RES) and 54% (STD) indicated that the growth of different trees was in response to common factors. Expressed population signal (EPS) is a measure of the agreement between the finite-sample chronology and the theoretical-population chronology based on an infinite number of trees [34], which varies from 0.0 to 1.0, and the threshold for accepting an EPS value is considered to be 0.85 [35]. The EPS of standard (STD) and residual (RES) chronologies both far exceed the threshold, indicating that the chronological datasets could very well represent the basic change characteristics of *L. chinensis* tree-ring radial growth. The mean correlations between trees is 0.49 (RES) and 0.48 (STD), the mean correlation within a tree is 0.60 (RES) and 0.62 (STD), and signal-to-noise ratios are 10.44 (RES) and 12.15 (STD); this reveals that the common growth limiting signals were contained in the tree-ring series. The first-order autocorrelation coefficient reflects the influence of climate conditions of the previous year on tree ring growth in the current year, and its value (0.51) in STD chronology denotes that the previous year's climate will impact the current year's growth of *L. chinensis*. Overall, the above statistical features suggest that the tree-ring width chronologies developed from *L. chinensis* are capable of further dendroclimatological analysis.

Since NDVI data are short in length and the RES chronology could preserve more high-frequency fluctuations by removing special early physiological conditions during the following growth years [23], while there is significant high frequency variation in NDVI due to its sensitivity to climate conditions [36]. We employed the RES chronology of Taibai mountain to clarify potential commonality between the tree-ring radial growth and the vegetation index. The adequacy of replication in the early years of the chronology was assessed with the sub-sample signal strength (SSS), which ensured the reliability of the reconstructed climate, as the sample size generally declines in the early stages of tree-ring

chronology [35]. To maximize the length of use of tree-ring chronologies and ensure the reliability of their reconstructions, we restricted our analysis to a period of signal strength above a threshold value of 0.75, which corresponds to a minimum sample depth of 7 cores. The period of the final chronologies was defined as AD 1868–2013.

3.3. Response of Tree-Ring Width to Climatic Factors

Single-month climatic parameters from the four surrounding stations shows consistent correlation patterns with the *L. chinensis* tree-ring width RES chronology in the time period of 1959–2013 (Figure 4). The RES chronology positively correlates with the monthly temperature, but negatively correlates with the monthly total precipitation, from February to June. To investigate the growth–climate response at a seasonal scale, we also performed correlation analysis between RES chronology and the seasonal combinations of the temperatures, and precipitation from the previous September to the current October. After calculation, the highest positive correlation ($r = 0.422$, $p < 0.01$) was found between chronology and the June–July mean temperature from Foping station; meanwhile, the highest negative correlation ($r = -0.347$, $p < 0.01$) was also found between the chronology and the March–June total precipitation from Foping station, indicating that summer temperatures and spring–summer precipitation were the main determinants of the final width of the tree-ring.

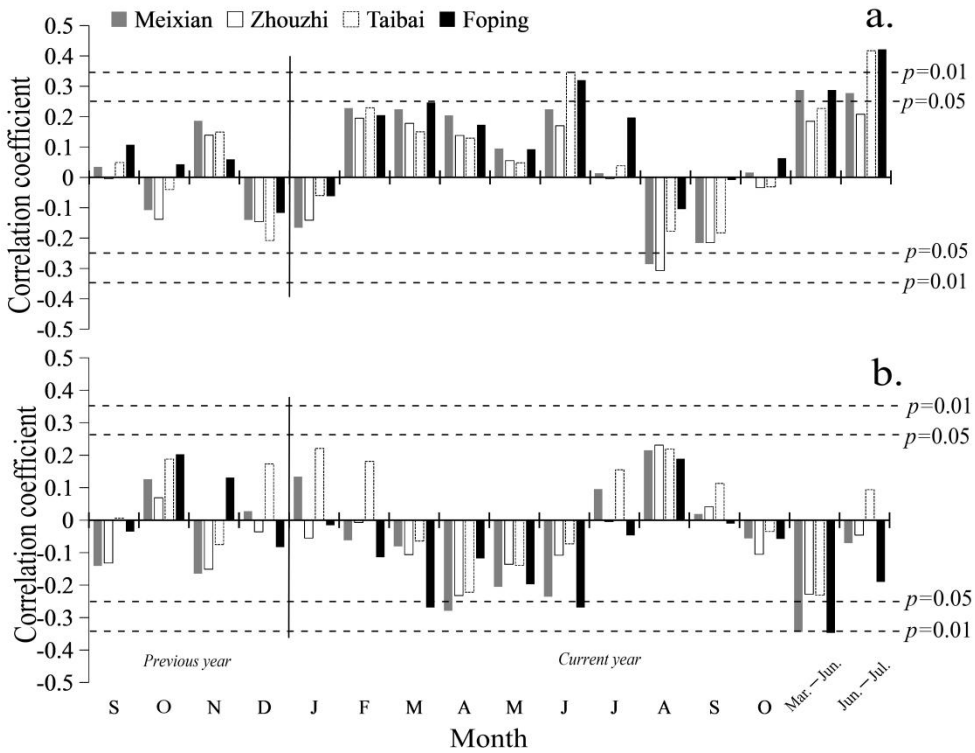


Figure 4. Correlation analysis between *Larix chinensis* tree-ring width residual chronology (RES) and monthly mean temperature (**a**) and total precipitation (**b**) from the Meixian, Zhouzhi, Taibai and Foping stations during 1959–2013.

3.4. Climate-NDVI and Growth-NDVI Relationships

We analyzed the correlations between the RES chronology and TBM NDVI (previous September to current December) as well as seasonal NDVI in AD 1991–2013. The chronology positively correlates with the monthly NDVI from January to October, but very significantly only in July ($r = 0.726$, $p < 0.01$), which is even higher than the highest correlation coefficient ($r = 0.582$, $p < 0.05$) between the June–July seasonal NDVI and RES chronology (Figure 5a). The scatter diagram indicates a clear correlation between RES chronology and July NDVI

(Figure 5b). Therefore, the July NDVI, which was also the annual maximum NDVI, was selected for further analysis.

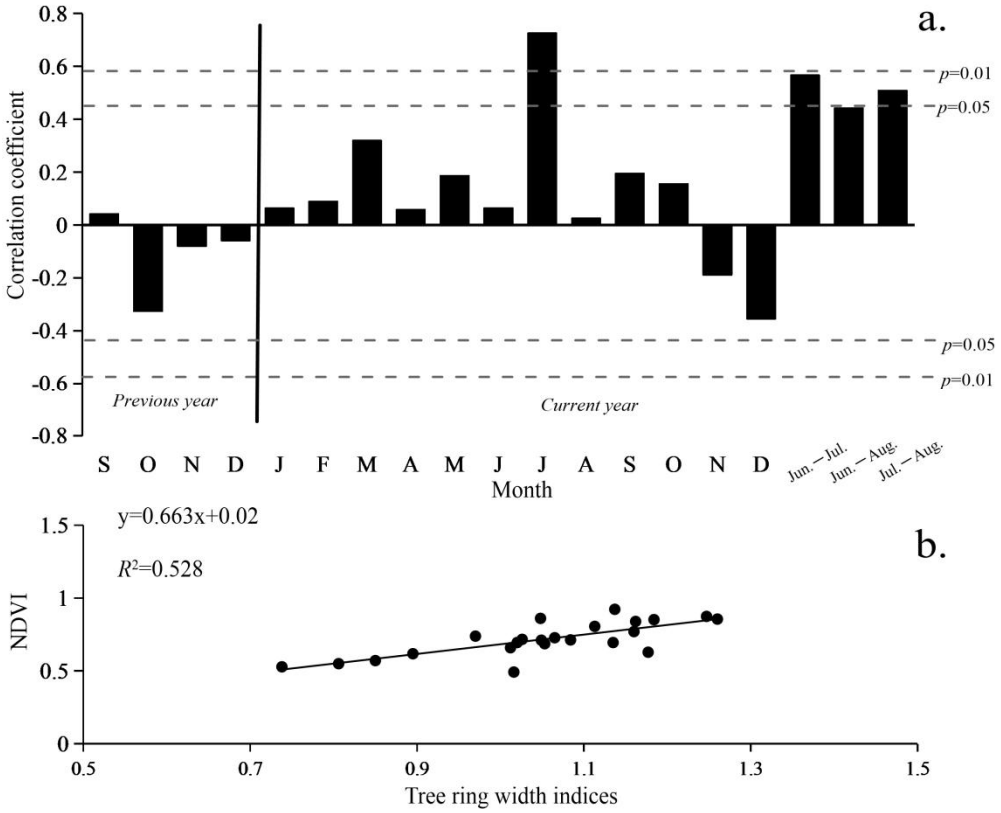


Figure 5. Correlation between TBM NDVI and residual chronology (RES) (**a**). Relationship between July NDVI and residual chronology (RES) during their common period of AD 1991–2013 (**b**).

Climate is one of the most important factors that control the variations in vegetation coverage, especially temperature and precipitation during the early growing season [37,38]. Since the variance exhibited by NDVI should be explained by using temperature, precipitation and other climatic variables [39–41], we performed a correlation analysis between TBM NDVI and the surrounding meteorological data. Close associations were found between the July NDVI and the surrounding climate conditions, and the local hydrothermal situation in the previous winter (January–February) and autumn (October–November) controlled the annual maximum vegetation coverage variation (Figure 6). Commonly, the monthly mean temperature and total precipitation in early spring and previous autumn at different stations considerably impacted the local vegetation dynamics in opposite ways. The highest positive correlation coefficient was found in the July NDVI with precipitation in the previous Oct. (r = 0.645, $p < 0.01$) from Zhouzhi station, and the previous October–November (r = 0.640, $p < 0.01$) from Taibai station. Meanwhile, the July NDVI was the most significantly and negatively correlated with temperatures in the previous October (r = −0.704, $p < 0.01$) and January–February (r = −0.637, $p < 0.01$) from Zhouzhi station.

These results indicate that: (1) the annual tree-ring width best correlates with the July NDVI; (2) statistically, hydrothermal condition in the previous later-autumn (especially October) and current early-spring (especially February) are the key factors driving the greenness of the *L. chinensis* forest canopy at Mt. Taibai.

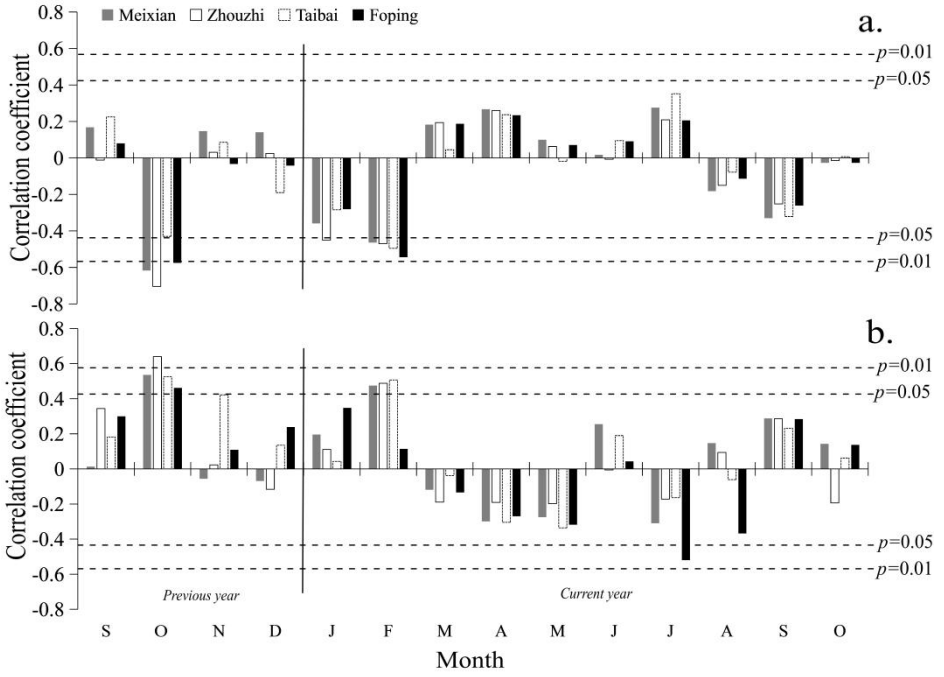


Figure 6. Correlation analysis between July NDVI and monthly mean temperature (**a**). Total precipitation (**b**) from the Meixian, Zhouzhi, Taibai and Foping stations during AD 1991–2013.

3.5. NDVI Reconstruction

According to the correlation analysis results above, the RES chronology was used to reconstruct the annual maximum NDVI variation of Mt. Taibai. We established the linear regression model between the *L. chinensis* tree-ring width RES chronology (X) and Mt. Taibai's July NDVI (Y), from AD 1991 to 2013. The transfer equation was designed as follows:

$$Y = 0.663 \times X + 0.02 \quad (1)$$

Equation (1) is reliable for the calibration period of AD 1991–2013, with the predictor variable accounting for 52.8% of the variance in the temperature (50.30% after adjusting for the loss of degrees of freedom). In model (1), the statistics are $n = 23$, $r = 0.726$, $F = 21.213$ and $p < 0.001$. Other main statistical items for leave-one-out cross-validation tests, such as sign test ($S1$), 1st-difference sign test ($S2$) and product mean test (t), are highly significant, and the rigorous cross-validation reduction of error (RE) test is positive, all indicating a reliable, stable and suitable model [33] (Table 3). The Durbin–Watson (D/W) value is 1.966, which is used to detect the presence of autocorrelation in the residuals from a regression analysis. When $n = 23$, a D/W value between 1.17 and 2.83 indicates that no autocorrelation within the series is detected [42]. Figure 7 shows the comparison between the estimated and actual July NDVI during 1991–2013.

Table 3. Leave-one-out cross validation statistics for the annual maximum NDVI reconstruction.

Period	*r*	R^2	R^2_{adj}	*S*1	*S*2	*RE*	*F*	*t*	*D*/*W*	*p*
1991–2013	0.726	52.80%	50.30%	18 (16 *,18 **)	16 (16 *,17 **)	0.523	21.213	2.36	1.966	<0.001

r—correlation coefficient; R^2—explained variance; R^2_{adj}—adjustment-explained variance; *S*1—sign test; *S*2—first difference sign test; *RE*—reduction of error; *t*—product mean test; *F*—variance test value; *D*/*W*—Durbin–Watson value. * significant at the 95% confidence level; ** significant at the 99% confidence level.

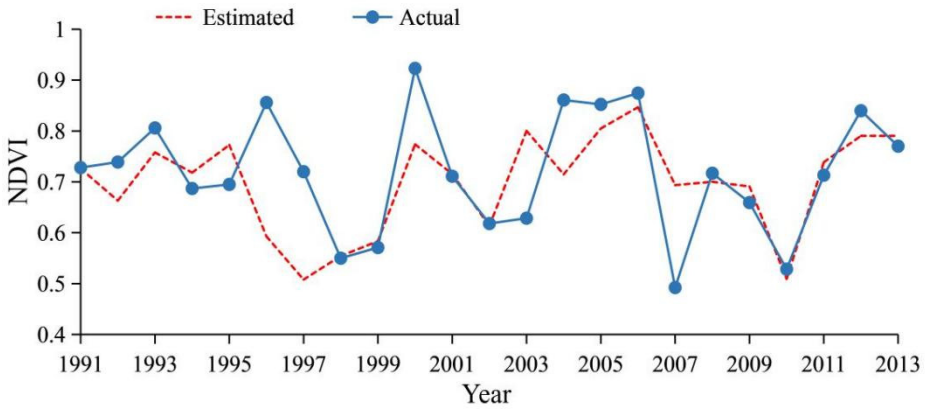


Figure 7. Comparison between the actual and estimated July NDVI during AD 1991–2013.

Based on Equation (1), we recovered the annual maximum NDVI series at the Mt. Taibai timberline as far back as 146 years (Figure 8), where the smoothed line is an 11-year moving average to demonstrate the low-frequency features of the reconstructed series, and to better observe the decadal-scale variation [43].

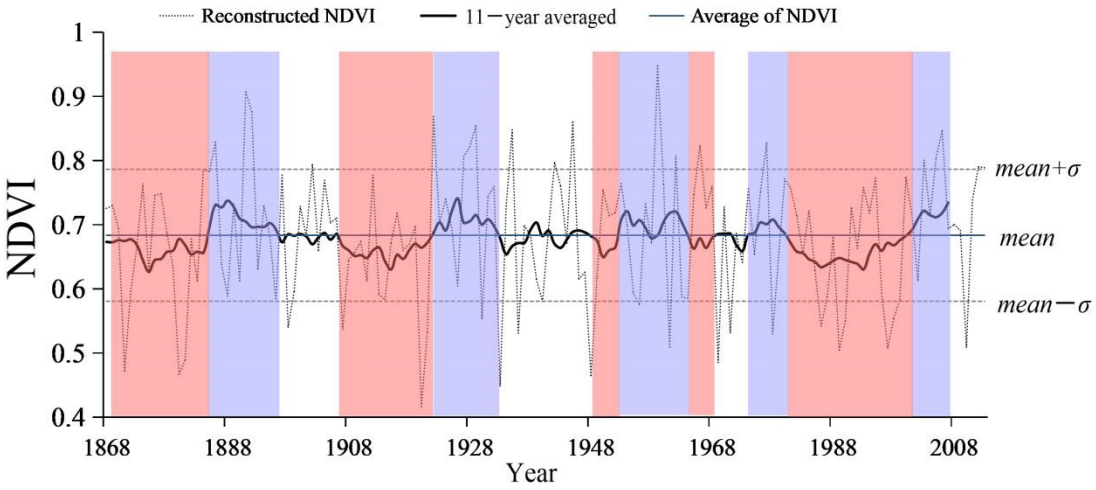


Figure 8. Variations of reconstructed annual maximum NDVI values of Mt. Taibai in AD 1849–2013. Blue bars are the dense vegetation-coverage periods, and the pink bars represent the sparse vegetation coverage periods according to the reconstructed curve from this paper.

Prominent fluctuations were detected in the last 146 years, and the high-frequency variation of the reconstructed NDVI at the Mt. Taibai timberline ranged from 0.416 to 0.947 (or mean ± standard deviation (σ) = 0.684 ± 0.102) over AD 1868–2013. The years in which the NDVI exceeded mean + σ (0.786) and dropped below the mean − σ (0.581) were defined as dense and sparse vegetation coverage years, respectively [44]. The dense and sparse coverage years accounted for 13.6% (20 years) and 16.4% (24 years), respectively, while normal vegetation density (mean NDVI from 0.581 to 0.786) occurred in a total of 102 years (69.9%) over the last 146 years. The top 10 most dense coverage years were 1891, 1892, 1922, 1928, 1929, 1935, 1945, 1959, 1966, 1977 and 2006, while the top 10 minimum NDVI years were 1920, 1933, 1948, 1961, 1969, 1971, 1978, 1989, 1997 and 2010. The low-frequency changes ranged from 0.631 to 0.742 throughout AD 1868–2013. Dense (sparse) years were defined as having an 11-year averaged value that was continuously higher (lower) than the long-term average (0.687). Generally, five dense coverage periods occurred in AD 1885–1896, 1922–1932, 1953–1964, 1974–1980 and 2001–2007 with a total duration of 49 years, and six sparse coverage periods occurred in AD 1868–1885, 1907–1921, 1933–1937, 1948–1952, 1965–1968 and 1981–2001 with a total duration of 65 years. The dominant dense

decades were the 1890s, 1930s, 1960s and 2000s, and the dominant sparse decades were the 1870s, 1920s, 1950s and 1990s.

3.6. Dryness/Wetness Index-NDVI Relationship

To evaluate the reliability of the reconstructed NDVI of Mt. Taibai and further confirm its representativeness, we compared it with the local dryness/wetness index (DWI) of the inverse vertical axis (to highlight the negative relationship between NDVI and DWI) at common intervals (Figure 9). Obviously, higher degree of DWI corresponds to lower NDVI, and vice versa. After smoothing using an 11-year moving average, a significant negative correlation was found between the reconstructed NDVI and DWI ($r = -0.221$, $p < 0.01$).

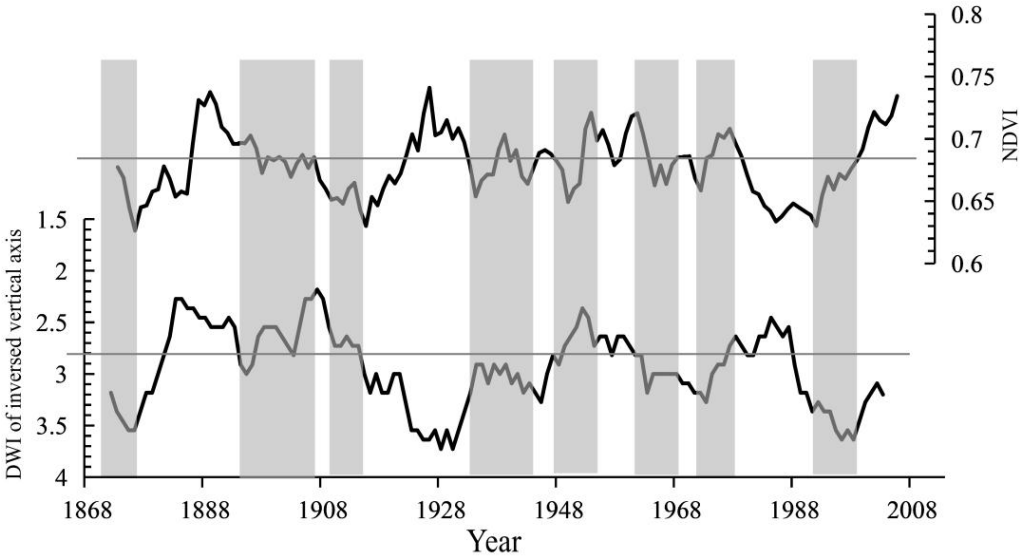


Figure 9. The 146a reconstructed annual maximum NDVI for Mt. Taibai and Baoji city dryness/wetness Index (DWI) of the inverse vertical axis. Vertical gray shading denotes the distinct periods of common trend.

3.7. NDVI Periodicity

Figure 10 displays the wavelet power spectral analysis over the reliable span of the tree-ring RES-chronology-based annual maximum NDVI reconstruction for Mt. Taibai, which exhibited clear multi-year and multi-decadal signals. As shown, the two most significant signals exist in the 7–11-year band for the 1870s–1900s and 1840s–1980s; and two significant signals exist in the 2–3/2–4-year band for the 1940s–1950s and 1960s–1980s. Meanwhile, signals in the 5–7-year band mainly exist between the 1920s and 1940s. Thus, the annual maximum NDVI of Mt. Taibai varies mainly on a multi-decadal scale [45].

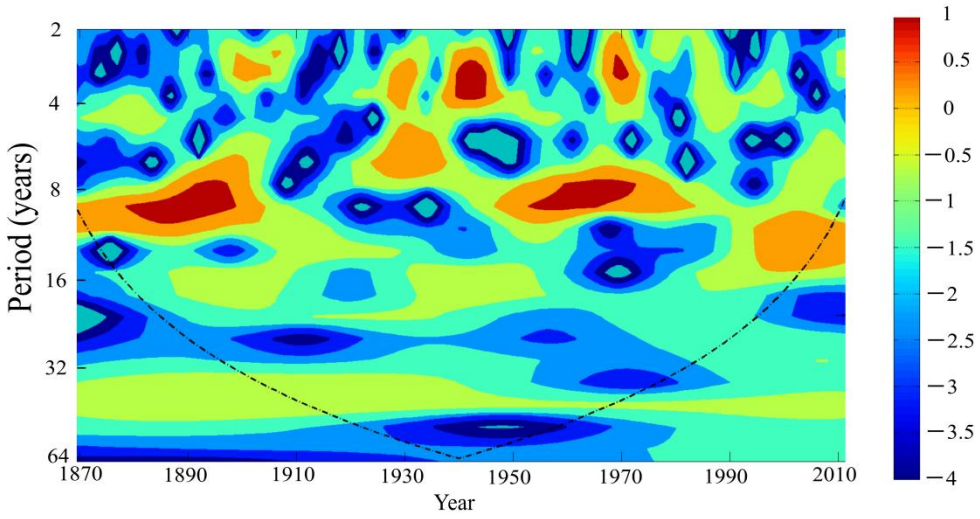


Figure 10. Wavelet power spectrum analysis plot for the *Larix chinensis* tree-ring width RES-chronology-based annual maximum NDVI reconstruction.

4. Discussion

4.1. Response Comparison among Climate, Tree-Ring Width and Greenness

4.1.1. Climate and Tree-Ring Width

Our study suggests that annual tree-ring width is mainly promoted by the growing season temperature while restrained by the corresponding period's precipitation. This finding is consistent with previous studies of other areas of the Qinling Mountains [46–48] and in accordance with the local geographical situation and plant physiology. The Qinling mountainous area has a generally high altitude, a humid climate, thick soil layer and high soil moisture content. When the temperature increases to the minimum temperature required for plant growth, the root system becomes active and the trees' cambium cells start to divide; his helps promote root and shoot growth, hence the lengthened growing season and the formation of early wood-wide rings [49,50]. During the early growing season, warmer temperatures help to induce earlier snowmelt and provide vital water availability, while higher precipitation may limit the soil moisture availability and the sunlight time, consequently slowing down the process of the photosynthesis [51]. Therefore, if excessive precipitation occurs during the growing season (especially March–June), tree growth is restrained, which results in a narrow ring.

4.1.2. Greenness and Tree-Ring Width

A number of investigations in North America and Eurasia [52–57] found a common signal that reflected the fundamental aspects of tree physiology among the NDVI of forest ecosystems: the tree-ring width and carbon isotope variation. As in this research, high correlation coefficients (Figure 5) indicate coherence between the satellite-derived Mt. Taibai July vegetation coverage and the actual *L. chinensis* radial growth. This remarkable result is largely coherent with previous conclusions that summer vegetation growth (June–August) correlates better with tree-ring width chronology [58,59]. The material source for tree-ring formation originates from the products of photosynthesis, which is mainly influenced by plant-canopy density and leaf density. The NDVI of Mt. Taibai reaches its peak in July when the vegetation coverage, density of the plant canopy, and leaf density are the lushest; therefore, the July NDVI had a critical impact on the final width of *L. chinensis* tree ring widths. In other words, the significant positive correlation results from common phenological processes and tree-ring radial growth are remarkably associated with the annual maximum NDVI at the Mt. Taibai timberline.

4.1.3. Greenness and Climate

The positive correlations between TBM NDVI and early-spring/late-autumn precipitation, and negative correlations between TBM NDVI and corresponding temperature, are reasonable. Because water availability in this region is related to thawing soil and melting snow-pack, autumn–winter precipitation/snow (August–April) enriches soil moisture storage and reduces the impacts of higher water loss through evaporation. Precipitation, which occurred in the current February, directly increases soil moisture availability and, thus, compensates for the soil water loss due to evaporation–transpiration; consequently, sufficient water supplement favors the summer surface NDVI. However, during early spring when vegetation begins to grow, water demand is increasingly higher. If precipitation is scarce and only meets the growth of drought-resistant plants, a number of moist–wet plants will decelerate or even stop growing, which leads to a lower summer surface NDVI. Thus, the July vegetation coverage of *L. chinensis* from this high-latitude semi-arid area is very sensitive to early-spring/late-autumn moisture deficiency and temperature anomalies. As reported, temperature showed a strong restraining effect on vegetation coverage during most of the previous and current growing seasons [52], suggesting that NDVI proxies indicate the physiological status of plants, and monthly precipitation from the previous summer to current autumn most remarkably impacts semi-arid and arid vegetation coverage [60].

4.2. Validation of the Reconstruction

4.2.1. The Representativeness of Reconstructed NDVI

To verify the reconstructed annual maximum NDVI, we investigated the consistency between the reconstructed NDVI series and environmental evolution in northern China, by comparing the dense and sparse periods discovered in this study with three NDVI reconstructions from the Qilian mountains [59], Badain Jaran Deserts [61] and Hulunbei'er steppe [58] during their common time intervals (Figure 11). In general, despite a few discrepancies such as the 1920s–1930s and 1980s–1990s—which may relate to different reconstructed time frames or site-specific NDVI anomalies—the severely dense periods of the 1890s–1900s, 1950s–1960s and 1970s–1980s and the sparse periods of the 1910s–1930s and 1960s–1970s identified in our study were also found in other studies; this indicates remarkable synchronized eco-environmental evolution between Mt. Taibai and other semi-arid and arid regions in north China.

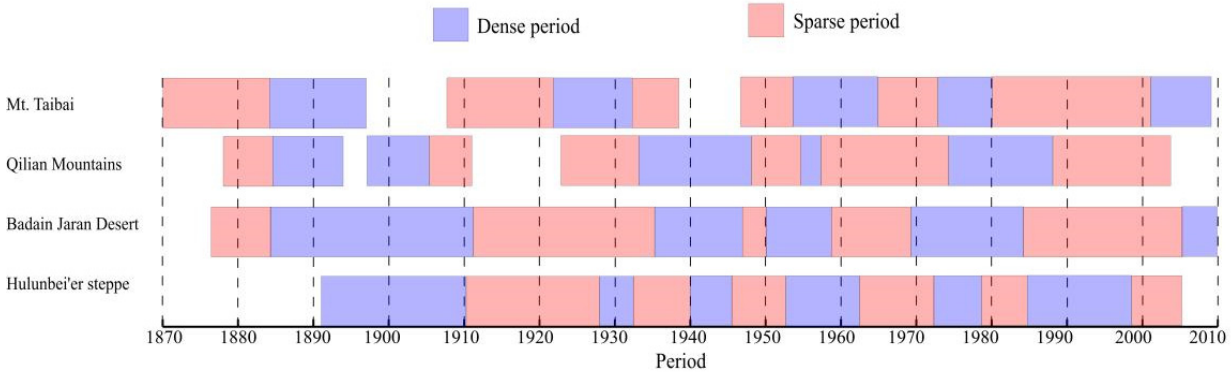


Figure 11. The dense and sparse periods of July NDVI in Mt. Taibai, June–August NDVI in the Qilian mountains [59], May–July NDVI in Badain Jaran Desert [61] and May–October NDVI in Hulunbei'er steppe [58].

4.2.2. Reconstructed NDVI and Local Dry/Humid Conditions

Previous research discovered that NDVI is a very good indicator of drought in arid environments [58], while local dryness/wetness indices and proxies, such as tree-ring, can be used to indicate and estimate typical NDVI variability in north China [60,62,63]. As shown in Figure 9, the sustained severe drought events, such as the high-DWI periods of

the 1880s, 1910s, 1940s, 1950s–1970s and 1980s–2010s, triggered extreme sparse vegetation periods, indicating that sparse greenness is associated with dry conditions. The sparse NDVI periods (1907–1921, 1965–1968 and 1981–2001) in our study agree well with the three drought events in high-incidence periods in Shaanxi (1915–1933, 1957–1977 and 1991–2002) in the 20th century [64]. A long-lasting sparse vegetation period occurred in 1868–1885, which corresponded to an extensive drought event (1876–1878) across China [65]. However, an abrupt positive correlation between the two series was, unexpectedly, found only during AD 1918–1930. Such discrepancies might be attributed to misrepresentations of historical facts, which may have led to unreliable dryness/wetness grading [66].

The significant and negative correlation between NDVI variations and the dryness/wetness index in the study area also prove that our reconstruction is reliable from another perspective. A relatively humid climate leads to better *L. chinensis* growth and thus improves the NDVI of this region, while NDVI is relatively lower under drought conditions.

4.3. Possible Climate Drivers

Wavelet power spectrum analysis demonstrates four main cycles of 2–3, 2–4, 5–7 and 7–11 years, respectively. The first three cycles are all within the typical El Niño–Southern Oscillation (ENSO) range [67], indicating the possible impact of ENSO on vegetation growth in the study area. ENSO events happening in different regions significantly affect the temperature and precipitation of Shaanxi province, thus impacting vegetation growth [68]. The 7–11-year cycle shows that regional vegetation growth may also affected by solar activity in addition to drought stress, and that it corresponds to the 11-year cycle of drought in northwest China [69].

5. Conclusions

In this paper, we found remarkable correlation coefficients ($r = 0.726$, $n = 23$, $p < 0.01$) between the *L. chinensis* tree-ring width's residual chronology and the 23-year integrated annual maximum NDVI datasets in Mt. Taibai, Qinling mountains. On this basis, a regression model was established to reconstruct the vegetation variations in Mt. Taibai in AD 1868–2013. The trans-function accounted for 52.8% of the observed NDVI variance in AD 1991–2013, indicating that the reconstructed NDVI series effectively tracks the observed data. Thus, we obtained a 146-year annual maximum NDVI series in Mt. Taibai to detect local vegetation dynamics and environmental evolution. The vegetation coverage in Mt. Taibai experienced five dense periods and six sparse periods, which are closely related to regional drought/humid conditions. Relatively humid climate improves regional NDVI, while NDVI is relatively lower under drought conditions. Moreover, the severely dense periods of the 1890s–1900s, 1950s–1960s and 1970s–1980s and the sparse periods of 1910s–1930s and 1960s–1970s identified in our study are also reported by previous studies in the Qilian mountains, Badain Jaran Deserts and Hulunbei'er steppe, indicating synchronized eco-environmental evolution between Mt. Taibai and other semi-arid and arid regions in north China. Based on the wavelet power spectrum analysis, four main cycles of 2–3, 2–4, 5–7 and 7–11 years can be found during the reliable periods. These multi-year and multi-decadal signals suggest a close teleconnection between regional vegetation variations and large-scale climate drivers, such as El Niño–Southern Oscillation.

Our study provides long-term scale data of annual maximum vegetation coverage fluctuations in Mt. Taibai, and indicates that vegetation in Mt. Taibai may be disturbed by both regional climate conditions and large climate drivers. Admittedly, NDVI reconstruction in this study is still limited, because it is based on *L. chinensis* tree cores from adjacent sampling sites and the calibration period is short in length; therefore, it is critical to develop a wide tree-ring network in the Qinling mountains, or even in all of northern China, and ameliorate the methods for the integration of existing NDVI datasets of different resolutions in the future. These conclusions may be helpful in extending the understanding of the relationship between tree growth and vegetation coverage, and will provide critical support to verify related study results.

Author Contributions: H.B. and J.Q. conceived and designed the experiments; J.Q. performed the experiments, analyzed the data and wrote the paper. P.Z., S.F., Y.X. and X.H. optimized the experiment and modified the manuscript. All authors have read and agreed to the published version of the manuscript.

Funding: This work was funded by the Public Welfare Special Fund of China Forestry Scientific Research (No. 201304309); the PhD early development program of Shangluo University (No. 18SKY005); the Natural Science Basic Research Program of Shaanxi Provincial Department of Science and Technology (No. 2021JQ-843); and the Natural Science Special Program of Shaanxi Provincial Department of Education (No. 20JK0616).

Institutional Review Board Statement: Not applicable.

Informed Consent Statement: Not applicable.

Acknowledgments: We thank the Taibai Mountain National Nature Reserve Administration for granting the license for sampling in the research area. We also thank the Disaster Supervising and Mechanism Modeling Key Laboratory of Shaanxi Province at the Baoji University of Arts and Sciences for supporting tree-ring width measurements and providing the pre-processing technology.

Conflicts of Interest: The authors declare no conflict of interest. The funding sponsors had no role in the design of the study, data collection, analyses, interpretation, writing of the manuscript, or in the decision to publish the results.

References

1. Yue, T.; Fan, Z. A review of responses of typical terrestrial ecosystems to climate change. *Chin. Sci. Bull.* **2014**, *59*, 217.
2. Piao, S.L.; Friedlingstein, P.; Ciais, P.; Zhou, L.; Chen, A. Effect of climate and CO_2 changes on the greening of the Northern Hemisphere over the past two decades. *Geophys. Res. Lett.* **2006**, *33*, 265–288. [CrossRef]
3. Zhao, Y.S. *Principle and Method of Remote Sensing Applied Analysis*; Science Press: Beijing, China, 2003.
4. Tucker, C.J.; Fung, I.Y.; Keeling, C.D.; Gammon, R.H. Relationship between atmospheric CO_2 variations and a satellite-derived vegetation index. *Nature* **1986**, *319*, 195–199. [CrossRef]
5. Tucker, C.J.; Sellers, P.J. Satellite remote sensing of primary production. *Int. J. Remote Sens.* **1986**, *7*, 1395–1416. [CrossRef]
6. Fang, J.Y.; Piao, S.L.; He, J.; Ma, W. Increasing terrestrial vegetation activity in China, 1982–1999. *Sci. China Ser. C* **2004**, *47*, 229–240.
7. Xin, Z.B.; Xu, J.X.; Zheng, W. Spatio-temporal variations of vegetation cover on the Chinese Loess Plateau (1981–2006): Impacts of climate changes and human activities. *Sci. China Ser. D* **2008**, *51*, 67–78. [CrossRef]
8. Wang, Q.; Chen, Y.; Ruan, X.R.; Li, X.D.; Wang, X.L.; Shi, J.Z.; Wang, Z.W. The changes of NDVI in China from 1982 to 2012 and its relationship with climatic factors. *Acta Agrestia Sin.* **2017**, *25*, 691–700.
9. Ljungqvist, F.C.; Piermattei, A.; Seim, A.; Krusic, P.J.; Esper, J. Ranking of tree-ring based hydroclimate reconstructions of the past millennium. *Quat. Sci. Rev.* **2020**, *230*, 106074. [CrossRef]
10. Cook, E.R.; Anchukaitis, K.J.; Buckley, B.M.; D'Arrigo, R.D.; Jacoby, G.C.; Wright, W.E. Asian monsoon failure and mega drought during the last millennium. *Science* **2010**, *328*, 486–489. [CrossRef]
11. Briffa, K.R.; Melvin, T.M.; Osborn, T.J.; Hantemirov, R.M.; Kirdyanov, A.V.; Mazepa, V.S.; Shiyatov, S.G.; Esper, J. Reassessing the evidence for tree-growth and inferred temperature change during the Common Era in Yamalia, northwest Siberia. *Quat. Sci. Rev.* **2013**, *72*, 83–107. [CrossRef]
12. Esper, J.; Cook, E.R.; Schweingruber, F.H. Low-frequency signals in long tree-ring chronologies for reconstructing past temperature variability. *Science* **2002**, *295*, 2250–2253. [CrossRef]
13. Liu, R.; Song, Y.; Liu, Y.; Li, X.; Song, H.; Sun, C.; Li, Q.; Cai, Q.; Ren, M.; Wang, L. changes in the tree-ring width-derived cumulative Normalized Difference Vegetation Index over northeast China during 1825 to 2013 CE. *Forests* **2021**, *12*, 241. [CrossRef]
14. Speer, J.H. Fine-scale ndvi reconstruction back to 1906 from tree-rings in the greater yellowstone ecosystem. *Forests* **2021**, *12*, 1324.
15. Qin, J.; BAI, H.Y.; Zhai, D.P.; Wang, J.; Li, S.H.; Li, B. The relationship between *Abies fargesii* tree-ring width and climate factors at Niubeiliang Natural Reserve in eastern Qinling Mountains of China. *J. Glaciol. Geocryol.* **2017**, *39*, 540–548. (In Chinese)
16. Qin, J.; Bai, H.Y.; Su, K.; Liu, R.J.; Zhai, D.P.; Wang, J.; Li, S.H.; Zhou, Q.; Li, B. Comparison of instrumental and interpolated meteorological data-based summer temperature reconstructions on Mt. Taibai in the Qinling Mountains, northwestern China. *Theor. Appl. Climatol.* **2018**, *133*, 633–645. [CrossRef]
17. Yan, B.; Yu, J.; Liu, Q.J.; Wang, L.H.; Hu, L.L. Tree-ring response of *Larix chinensis* on regional climate and sea-surface temperature variations in alpine timberline in the Qinling Mountains. *J. For. Res.* **2020**, *31*, 209–218. [CrossRef]
18. Zhang, Y.X.; Hu, Y.X.; Zhang, B.; Li, Y.X.; Zhang, X.Y.; Xie, Y. Conflict between nature reserves and surrounding communities in China: An empirical study based on a social and ecological system framework. *Glob. Ecol. Conserv.* **2019**, *21*, e00804. [CrossRef]
19. Fang, K.; Yang, B.; Zheng, H. Research methods of dendrochronology and its application in global change. *Quat. Sci.* **2015**, *35*, 1283–1293. (In Chinese)

20. Stokes, M.A.; Smiley, T.L. *An Introduction to Tree Ring Dating*; University of Chicago Press: Chicago, IL, USA, 1968.
21. Holmes, R.L. *Dendrochronology Program Library Users Manual. Laboratory of Tree-Ring Research*; University of Arizona: Tucson, AZ, USA, 1994.
22. Cook, E.R.; Krusic, P.J. Program ARSTAN. In *A Tree-Ring Standardization Program Based on Detrending and Autoregressive Time Series Modeling, with Interactive Graphics*; Lamont-Doherty Earth Observatory of Columbia University: Palisades, NY, USA, 2005.
23. Fritts, H.C. *Tree Rings and Climate*; Academic Press: New York, NY, USA, 1976.
24. Monserud, R.A. Time-series analyses of tree-ring chronologies. *For. Sci.* **1986**, *32*, 349–372.
25. Cook, E.R. A Time Series Analysis Approach to Tree Ring Standardization. Ph.D. Thesis, University of Arizona, Tucson, AZ, USA, 1985.
26. Ma, X.P.; Bai, H.Y.; He, Y.N.; Qin, J. The vegetation remote sensing phenology of Qinling Mountains based on NDVI and its response to temperature: Taking with the territory of Shaanxi as an example. *Scientia. Geograph. Sin.* **2015**, *35*, 1616–1621.
27. Qi, G.Z.; Bai, H.Y.; Meng, Q.; Zhao, T.; Guo, S.Z. Reconstruction of spring dry and wet changes in Taibai Mountain area based on tree ring width. *Arid Land Geogr.* **2020**, *43*, 955–966.
28. Michaelsen, J. Cross-validation in statistical climate forecast models. *J. Clim. Appl. Meteor.* **1987**, *26*, 1589–1600. [CrossRef]
29. Liu, N.; Zhou, Q.; Bao, G. Droughts and broad-scale climate variability reflected by temperature-sensitive tree growth in the Qinling mountains, central china. *Int. J. Biometeorol.* **2013**, *57*, 169–177. [CrossRef] [PubMed]
30. Torrence, C.; Compo, G.P. A practical guide to wavelet analysis. *Bull. Am. Meteorol. Soc.* **1998**, *79*, 61–78. [CrossRef]
31. Tucker, C.J.; Slayback, D.A.; Pinzon, J.E.; Los, S.O.; Myneni, R.B.; Taylor, M.G. Higher northern latitude normalized difference vegetation index and growing season trends from 1982 to 1999. *Int. J. Biometeorol.* **2001**, *45*, 184–190. [CrossRef]
32. Lucht, W.; Prentice, I.C.; Myneni, R.B.; Sitch, S.; Friedlingstein, P.; Cramer, W.; Bousquet, P.; Buermann, W.; Smith, B. Climatic control of the high-latitude vegetation greening trend and Pinatubo effect. *Science.* **2002**, *296*, 1687–1689. [CrossRef]
33. Cook, E.R.; Kairiukstis, L.A. *Methods of Dendrochronology Applications in the Environmental Sciences*; Kluwer Academic Publishers: Dordrecht, The Netherlands, 1990.
34. Briffa, K.R. Interpreting high-resolution proxy climate data: The example of dendroclimatology. In *Analysis of Climate Variability: Applications of Statistical Techniques*; Von Storch, H., Navarra, A., Eds.; Springer: Berlin/Heidelberg, Germany, 1995; pp. 77–94.
35. Wigley, T.M.L.; Briffa, K.R.; Jones, P.D. On the average value of correlated time-series, with applications in dendroclimatology and hydrometeorology. *J. Appl. Meteorol.* **1984**, *23*, 201–213. [CrossRef]
36. Li, J.J.; Wang, S.; Qin, N.S.; Liu, X.S.; Jin, L.Y. Vegetation index reconstruction and linkage with drought for the source region of the Yangtze river based on tree-ring data. *Chin. Geogr. Sci.* **2021**, *31*, 684–695. [CrossRef]
37. Ding, M.J.; Zhang, Y.L.; Liu, L.S.; Zhang, W.; Wang, Z.F.; Bai, W.Q. The relationship between NDVI and precipitation on the Tibetan Plateau. *J. Geogr. Sci.* **2007**, *17*, 259–268. [CrossRef]
38. Zeng, B.; Yang, T.B. Impacts of climate warming on vegetation in Qaidam Area from 1990 to 2003. *Environ. Assess.* **2008**, *144*, 403–417. [CrossRef]
39. Schultz, P.A.; Halpert, M.S. Global correlation of temperature, NDVI and precipitation. *Adv. Space Res.* **1993**, *13*, 277–280. [CrossRef]
40. Tucker, C.J. Red and photographic infrared linear combinations for monitoring vegetation. *Remote Sens. Environ.* **1979**, *8*, 127–150. [CrossRef]
41. Tucker, C.J.; Pinzon, J.E.; Brown, M.E.; Slayback, D.A.; Pak, E.W.; Mahoney, R.; Vermote, E.F.; El Saleous, N. An extended AVHRR 8-km NDVI dataset compatible with MODIS and SPOT vegetation NDVI data. *Int. J. Remote Sens.* **2005**, *26*, 4485–4498. [CrossRef]
42. Durbin, J.; Watson, G.S. Testing for serial correlation in least squares regression I. *Biometrika* **1951**, *38*, 159–178. [CrossRef]
43. Jiang, Y.; Yuan, X.; Zhang, J.; Han, S.; Chen, Z.; Wang, X.; Wang, J.; Hao, L.; Li, G.; Dong, S.; et al. Reconstruction of June–July Temperatures Based on a 233 Year Tree-Ring of *Picea jezoensis var. microsperma*. *Forests* **2019**, *10*, 416. [CrossRef]
44. Bao, G.; Liu, Y.; Liu, N. A tree-ring-based reconstruction of the Yimin River annual runoff in the Hulun Buir region, Inner Mongolia, for the past 135 years. *Chin. Sci. Bull.* **2013**, *57*, 4765–4775. [CrossRef]
45. Li, T.; Li, J.; Au, T.F.; Zhang, D.D. Tree-ring width data of *Tsuga longibracteata* reveal growing season temperature signals in the North-Central pearl river basin since 1824 AD. *Forests* **2021**, *12*, 1067. [CrossRef]
46. Liu, Y.; Linderholm, H.W.; Song, H.; Cai, Q.; Tian, Q.; Sun, J.; Chen, D.; Simelton, E.; Seftigen, K.; Tian, H.; et al. Temperature variations recorded in *Pinus tabulaeformis* tree rings from the southern and northern slopes of the central Qinling Mountains, central China. *Boreas* **2009**, *38*, 285–291. [CrossRef]
47. Kang, Y.X.; Liu, J.H.; Dai, S.F.; He, X.J. Characteristics of ring-width chronologies of *Larix chinensis* and their responses to climate change at different elevations in Taibai Mountain. *J. Northwest Univ. A&F Nat. Sci. Ed.* **2010**, *38*, 141–147. (In Chinese)
48. Dang, H.S.; Jiang, M.X.; Zhang, Q.F.; Zhang, Y.J. Growth responses of subalpine fir (*Abies fargesii*) to climate variability in the Qinling Mountain, China. *Forest Ecol. Manag.* **2007**, *240*, 143–150. [CrossRef]
49. Graumlich, L.J. Subalpine tree growth, climate, and increasing CO_2: An assessment of recent growth trends. *Ecology* **1991**, *72*, 1–11. [CrossRef]
50. Sheppard, P.R.; Graumlich, L.J.; Conkey, L.E. Reflected-light image analysis of conifer tree rings for reconstructing climate. *Holocene* **1996**, *6*, 62–68. [CrossRef]
51. Vaganov, E.A.; Hughes, M.K.; Kirdyanov, A.V.; Schweingruber, F.H.; Silkin, P.P. Influence of snowfall and melt timing on tree growth in subarctic Eurasia. *Nature* **1999**, *400*, 149–151. [CrossRef]

52. Kaufmann, R.K.; D'Arrigo, R.D.; Laskowski, C.; Myneni, R.B.; Zhou, L.M.; Davi, N.K. The effect of growing season and summer greenness on northern forests. *Geophys. Res. Lett.* **2004**, *31*, 3–6. [CrossRef]
53. D'Arrigo, R.D.; Malmstrom, C.M.; Jacoby, G.C.; Los, S.O.; Bunker, D.E. Correlation between maximum latewood density of annual tree rings and NDVI based estimates of forest productivity. *Int. J. Remote Sens.* **2000**, *21*, 2329–2336. [CrossRef]
54. Wang, J.; Rich, P.M.; Price, K.P.; Kettle, W.D. Relations between NDVI and tree productivity in the central Great Plains. *Int. J. Remote Sens.* **2004**, *25*, 3127–3138. [CrossRef]
55. Chiesi, M.; Maselli, F.; Bindi, M.; Fibbi, L.; Cherubini, P.; Arlotta, E.; Tirone, G.; Matteucci, G.; Seufert, G. Modelling carbon budget of Mediterranean forest using ground and remote sensing measurements. *Agric. Forest Meteorol.* **2005**, *135*, 22–34. [CrossRef]
56. Lopatin, E.; Kolstrom, T.; Spiecker, H. Determination of forest growth trends in Komi Republic (northwestern Russia): Combination of tree-ring analysis and remote sensing data. *Boreal Environ. Res.* **2006**, *11*, 341–353.
57. Leavitt, S.W.; Chase, T.N.; Rajagopalan, B.; Lee, E.; Lawrence, P.J. Southwestern US tree-ring carbon isotope indices as a possible proxy for reconstruction of greenness of vegetation. *Geophys. Res. Lett.* **2008**, *35*, 150–152. [CrossRef]
58. Chen, Z.J.; Li, J.B.; Fang, K.Y.; Davi, N.K.; He, X.Y.; Cui, M.X.; Zhang, X.L.; Peng, J.J. Seasonal dynamics of vegetation over the past 100 years inferred from tree rings and climate in Hulunbei'er steppe, northern China. *J. Arid Environ.* **2012**, *83*, 86–93. [CrossRef]
59. Wang, W.Z.; Liu, X.H.; Chen, T. Reconstruction of regional NDVI using tree-ring width chronologies in the Qilian Mountains, northwestern China. *Chin. J. Plant Ecol.* **2010**, *34*, 1033–1044.
60. Liang, E.Y.; Shao, X.M.; He, J.C. Relationships between tree growth and NDVI of grassland in the semiarid grassland of north China. *Int. J. Remote. Sens.* **2005**, *26*, 2901–2908. [CrossRef]
61. Chen, F.; Yuan, Y.J.; Zhang, R.B.; Yu, S.L. Reconstruction of regional NDVI using tree-ring width chronology in the southern edge of the Badain Jaran desert, northwestern China. *Desert Oasis Meteor.* **2015**, *9*, 1033.
62. He, J.; Shao, X. Relationships between tree-ring width index and NDVI of grassland in Delingha. *Chin. Sci. Bull.* **2006**, *51*, 1106–1114.
63. Liang, E.Y.; Shao, X.M.; Xu, Y. Tree-ring evidence of recent abnormal warming on the southeast Tibetan Plateau. *Theor. Appl. Climatol.* **2009**, *98*, 9–18. [CrossRef]
64. Li, H.M.; Fan, J.Z.; Li, X.M. Preliminary analysis of extreme drought events in Shaanxi province during the past 500 years. *J. Shaanxi Meteorol.* **2011**, 35–37. (In Chinese)
65. Zhang, D.E.; Liang, Y.Y. A long lasting and extensive drought event over China in 1876–1878. *Adv. Clim. Chang. Res.* **2010**, *1*, 91–99. (In Chinese) [CrossRef]
66. Wang, Y.J.; Ma, Y.Z.; Lu, R.J.; Gao, S.Y. Summer NDVI variability recorded by tree radial growth in the Xinglong Mountain, the eastward extension of the Qilian Mountains, since 1845 AD. *Geograph Res.* **2016**, *35*, 653–663.
67. Allan, R.; Lindesay, J.; Parker, D. *El Niño-Southern Oscillation and Climatic Variability*; CSIRO Publishing: Melbourne, Australia, 1996.
68. Zhang, C.; Zhao, J.B. Effects of El Niño-Southern Oscillation events on climate in Shaanxi province. *J. Shaanxi Normal Univ.* **2010**, *38*, 98–104.
69. Cai, Q.F.; Liu, Y. January to August temperature variability since 1776 inferred from tree-ring width of *Pinus tabulaeformis* in Helan Mountain. *J. Geogr. Sci.* **2007**, *17*, 293–303. [CrossRef]